DEVELOPMENT OF THREE-DIMENSIONAL TOMOGRAPHY METHOD FOR ANALYSIS OF DROPLET BEHAVIOR

X.H. NGUYEN[1], S.H. LEE[1], D.H. SHIN[1], H.S. KO[2,c]

[1]Graduate School of Mechnical Engineering, Sungkyunkwan University, Suwon, Korea
[2]School of Mechnical Engineering, Sungkyunkwan University, 300 Cheoncheon-dong, Jangan-gu, Suwon, Gyeonggi-do 440-746, Korea

[c]Corresponding author: Tel.: 82-31-290-7453; Fax: 82-31-290-5889 ; Email: hanseoko@skku,edu

KEYWORDS:
Main subjects: flow visualization and control
Fluid: water droplet
Visualization method: tomographic particle image velocimetry
Other keywords: tomography, electrohydrodynamic jetting

ABSTRACT: Three-dimensional optical tomography techniques have been developed to reconstruct three-dimensional objects using a set of two-dimensional projection images. A blob method using several basis functions such as a cubic cosine basis function, a cubic B-spline basis function and a Gaussian basis function have been used to calculate the weighting coefficients for the projection matrix. The multiplicative algebraic reconstruction technique (MART) has also been used to solve the inverse problem. The reconstructing program has been examined by using several phantoms including droplet behaviors and random distributions of particles in a volume. The three dimensional volume of particles has been reconstructed from four projections which are positioned with an offset angle of 45° between each others. Then, the three-dimensional velocity fields has been obtained from the reconstructed particle volumes by the three-dimensioanl cross correlation. The velocity field of the synthetic vortex flow has been reconstructed to analyze the three-dimensional tomography algorithm.

1. Introduction

The observation of the ejection of the liquids from the electrostatic nozzle under high applied voltages is interesting subject due to its various behaviors in jetting and its widespread application in industry such as ink-jet printing, drug delivery and encapsulation [1-3] Formation of droplet occurs in many states depending on the applied voltages for the nozzle. It can be divided into stable and unstable states with different pendant droplet menisci, droplet sizes, and formation frequency. In stable states, droplets are formed in dripping and micro dripping modes while they are formed in pulse, spindle and multi-jet states in unstable states [4]. Thus, a non-intrusive measurement is an appropriate method for analysis of droplet formation with numbers, sizes and locations of droplets as well as flow behaviors inside an ejected droplet.

Tomography is a method of reconstructing an object from its multidirectional projection data. The projection data which represent the line or ray integral of the unknown function measured along given directions is achieved from the radiation-based and optical-based measurement such as laser interferometry, X-ray attenuation, ultrasonics-based non-destructive evaluation and light intensity using optoelectronic sensor as a charge coupled device (CCD) [5, 6]. These data measurement proposes that the tomography method is the effective tools of the non-invasive and quantitative measurements of thermal and fluid flows [7]. The spatial distribution of the properties about the object can be reconstructed from the line integrals of the properties by the computerized tomography technique.

The projection data can be obtained by the integral method along the incident direction as follows:

$$\psi(s,\theta) = \int_{-\infty}^{+\infty} f(x,y)dt \qquad (1)$$

where, $\psi(s,\theta)$ is the projection data, and $f(x,y)$ is the object function that represents the object to be reconstructed, which is integrated along the coordinate axis t. The Cartesian coordinate system (s,t) is rotated at angle θ relative to the basic coordinate system (x,y) (Fig. 1 (a)). The actual reconstructed problems in an industry have one distinguishing characteristics which is different from the medical treatment. They are limited-data problems as usual and it is often

impossible to obtain the projection data from the object at all angles because of the limited space and economy. In order to reconstruct acceptable results from the limited projection data, the algebraic reconstruction technique (ART) and the multiplicative algebraic reconstruction technique (MART) were proposed [8-10].

In this study, the three-dimensional optical tomography reconstruction technique was investigated with several manners of building the projection matrix. The algorithm considers the projection data as the image intensities captured by CCD cameras. Each pixel is a ray or line-of-sight and the intensity in each pixel is the integral along this line-of-sight of the object's intensity in three-dimensional volume or voxels. The unknown intensities of voxels were reconstructed from the two-dimensional images in several camera views. The MART was used in combining with three different basis functions for building projection matrix. The algorithm was examined with two kinds of phantom which were the phantom of droplet behaviors and the phantom of random distribution of particles inside a volume. The performance of the algorithm was investigated to reconstruct the particle field for the three-dimensional cross correlation to obtain the three-dimensional velocity field by a tomographic particle image velocitymetry technique [11, 12].

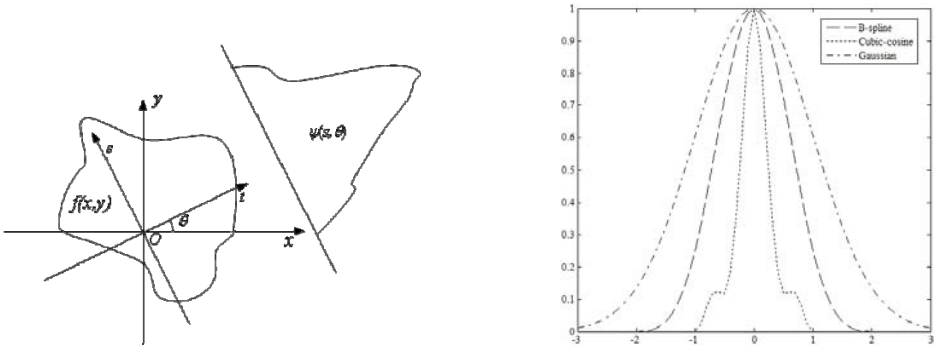

(a) Cross-sectional field and its projection (b) Distribution of basis functions

Fig. 1 Projection of field along ray and basis functions

2. Tomographic reconstruction technique

2.1 Formulation of algebraic reconstruction technique

For a three-dimensional test field, one can represent the field as a series of basis functions allowing their parameters to be optimally determined. The location of each basis function is given as [7]

$$\hat{f}(x,y,z)=\sum_{j=1}^{N} O_j b(x-x_j, y-y_j, z-z_j) \tag{2}$$

where $\hat{f}$ is an object function that represents the field to be reconstructed, b is a general form of the basis function located at (x_j,y_j,z_j), and O_j is the height coefficient of the j-th basis function centered at a fixed location of (x_j,y_j,z_j). If $\hat{f}$ is the three-dimensional intensity distribution or an array of unknown voxels, the pixel intensity of the recorded two-dimensional images is the integration of $\hat{f}$ along the line-of-sight on pixels obtained from a calibration procedure. From Eqs. (1) and (2), the *i-th* measurement data can be expressed as follows [9, 10]:

$$\psi_i \approx \int_{ti} \hat{f}(x,y,z)dt \approx \sum_{j=1}^{N} O_j \int_{ti} b_i(x-x_j, y-y_j, z-z_j)dt = \sum_{j=1}^{N} O_j W_{ij} \tag{3}$$

which in matrix form is

$$\psi_i = W_{ij} O_j \tag{4}$$

where *W* is the projection matrix which its weighting coefficients represent the contribution of each voxel to a pixel and depend on a factor of camera orientation or projection direction and measurement volume configuration. The matrix *W* has dimensions (number of pixel or ray) *x* (number of voxels or basis functions). Since each line-of-sight or ray on a pixel just intersects with small number of basis functions or voxels, the projection matrix is very sparse. Thus, the tomography technique is to estimate the unknown O_j or solve the linear system equation. An optimized set of these unknowns must be found to minimize the deviations between the virtual projection $\hat{\psi}$ of an intermediate object function $\hat{f}$ and the measured projection ψ of the actual field *f*.

2.2 Basis functions for building projection matrix

Beside the factors of projection orientation and the measured volume configuration, the choice of the basis function centered at the fixed locations also effects on the weighting coefficients of the projection matrix. A pixel line-of-sight arisen from a 2D projection will intersect some unknown voxels in the volume of field. The distance from the centers of the voxels to the line-of-sight will be used to calculate the weighting values of the projection matrix according to the basis function. The use of a smooth basis function can accurately represent a relatively smooth object field with far fewer coefficients (unknowns) than with the square-pixel basis function.

Three different sets of local basis functions as Gaussian, cubic B-spline and cubic cosine were evaluated for the tomographic reconstruction. The Gaussian basis function which can be formulated as [11, 12]:

$$\begin{aligned} b(d_j) &= e^{-\frac{|d_j|^2}{2\sigma^2}}, & |d_j| \le \Delta \\ &= 0, & |d_j| > \Delta \end{aligned} \qquad (5)$$

In this case, Δ is the diameter of the blob centered at the fixed location in the volume of field and equals to the variance σ.

Another one of comparative studies for the choice of basis functions suggests the use of the cubic B-spline [13], described by

$$\begin{aligned} b(d_j) &= \frac{\left(2\Delta - |d_j|\right)^3 - 4\left(\Delta - |d_j|\right)^3}{4\Delta^3}, & |d_j| < \Delta \\ &= \frac{\left(2\Delta - |d_j|\right)^3}{4\Delta^3}, & \Delta \le |d_j| \le 2\Delta \\ &= 0, & 2\Delta < |d_j| \end{aligned} \qquad (6)$$

where Δ is the grid spacing, d_j is the distance from a center of a voxel to the ray.

Finally, the cubic cosine function can be described as follow [14, 15 and 19]:

$$\begin{aligned} b(d_j) &= \frac{12\pi^2}{(5\pi^2+16)}\left[\begin{array}{l}\left(\frac{1}{3} - |d_j|^2\right)\left(1 + \frac{1}{4}\cos 3\pi|d_j|\right) \\ + \frac{|d_j|}{4\pi}\sin 3\pi|d_j| + \frac{2}{3\pi^2}\left(1 + \cos 3\pi|d_j|\right)\end{array}\right], & |d_j| < \frac{1}{3}\Delta \\ &= \frac{24\pi^2}{(5\pi^2-16)}\left[\begin{array}{l}0.5\left(|d_j| - 1\right)^2\left(1 + \frac{1}{4}\cos 3\pi|d_j|\right) \\ + \frac{3(1-|d_j|)}{8\pi}\sin 3\pi|d_j|\end{array}\right], & \frac{1}{3}\Delta \le |d_j| \le \Delta \\ &= 0, & \Delta < |d_j| \end{aligned} \qquad (7)$$

A sketch of all of three basis functions is shown in Fig. 1 (b) in which the cubic B-spline and Gaussian are smoother than the cubic cosine. All of these functions were applied and tested for the developed tomography methods in this study.

2.3 Multiplicative algebraic reconstruction technique (MART)

In the linear system Eq. (4), the weighting values of W_{ij} are known and the projection data ψ_I are obtained from the experimental measurements as light intensity from CCD camera. The problem of reconstruction is one of inverting the matrix W_{ij} to find O_j. Due to the limitation of the projection data, the iterative tomographic algorithms are adopted. These algorithms are divided into two types based on the method of updating corrections for the field variables. The correction that is additive referred to as an additive reconstruction technique is the ART (algebraic reconstruction technique) and the correction that is multiplicative referred to as a multiplicative algebraic reconstruction technique is the MART [6]. Thus, the MART algorithm differs from the ART algorithm only in the way the deviation between the virtual projection $\hat{\psi}_i$ and the measured projection ψ_I are distributed among the object coefficients.

In this study, the MART which was proposed by Gordon and Herman et al. [9-11] was used. It is described as followings:

$$O^{q+1} = O^q \left[\frac{\psi_i}{\hat{\psi}_i} \right]^{\mu W_{i,j}} = O^q \left[\frac{\psi_i}{\sum_{j=1}^{N} W_{i,j} O^q} \right]^{\mu W_{i,j}} \tag{8}$$

where, μ is relaxation parameter which is equal to *1* in this study. One advantage of using MART is to ensure a non-negative object field in reconstructing non-negative scalar.

3. Computer-synthesized phantom and reconstruction performance

3.1 Computer-synthesized phantom of droplet distribution

In order to investigate the reliability and quality, the MART algorithm with several basis functions for building projection matrix were evaluated numerically. The two 3D phantoms with three and four droplets distribution were synthesized respectively. The first phantom constructs one big droplet and other three small droplets, which can be expressed mathematically in Eq. (9) as shown in Fig. 2 (a). The second phantom is composed of three different sized droplets Eq. (10) as shown in Fig. 2 (b) [15]. The droplets are distributed in the volume size of *15x15x15 (units)*. The normalized field impedance is 0 for the region outside the droplet and 1 for the region inside the droplet.

$$f_1(x,y,z) = \begin{cases} 1, & (x-0.3)^2 + (y-0.3)^2 + (z-0.1)^2 \le 0.1^2 \\ 1, & \left(x - \frac{y+0.1}{5}\right)^2 + \left(y - \frac{z+0.5}{4}\right)^2 + \frac{z}{12} \;\&\; z \le 0 \\ 1, & (x+0.2)^2 + (y-0.3)^2 + (z+0.1)^2 \le 0.08^2 \\ 1, & (x-0.1)^2 + (y)^2 + (z-0.1)^2 \le 0.1^2 \\ 0, & \text{otherwise} \end{cases} \tag{9}$$

$$f_2(x,y,z) = \begin{cases} 1, & (x-0.15)^2 + (y-0.15)^2 + z^2 \le 0.2^2 \\ 1, & (x+0.3)^2 + (y+0.3)^2 + (z+0.1)^2 \le 0.15^2 \\ 1, & (x-0.1)^2 + (y+0.3)^2 + (z-0.1)^2 \le 0.1^2 \\ 0, & \text{otherwise} \end{cases} \tag{10}$$

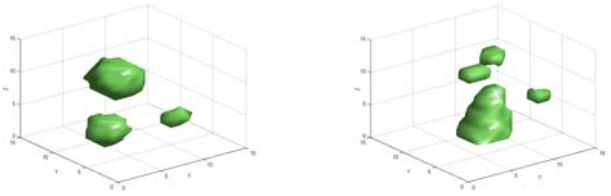

(a) Distribution of three droplets (b) Distribution of four droplets

Fig. 2 Synthetic phantoms of droplets

3.2 Computer-synthesized phantom of particle random distribution

Recent years, tomographic method has been used to reconstruct the volume of particle immersed in the flow field from several two-dimensional images captured by CCD cameras. The two volumes will be used to obtain the velocity field by a cross-correlation method. This working principle is called tomographic particle image velocimetry (Tomo-PIV) proposed by Elsinga et al. [11]. Thus, the tomography method combining with several basis functions introduced in this study was also examined using the synthesized phantom simulating the random distribution of particles in a volume. These are the random *N*-peaks Gaussian distribution which is shown as follows:

$$f_3(x,y,z)=\sum_{j=1}^{N}\frac{I_{\max}}{4\pi^2 d^3}\left(\exp(-\frac{0.5(x-x_j)^2-0.5(y-y_j)^2-0.5(z-z_j)^2}{d^2})\right) \qquad (11)$$

where, I_{max} is the maximum intensity, N is number of particle, (x_j,y_j,z_j) are the centers of particle and d is the diameter of the particle. The *2580* particles were distributed randomly in the volume with size of *255x255x41* voxels. The maximum intensity was also chosen randomly from 1 to 100 as gray level. Using this random particle as the first position, the second position was created by calculating the displacement of each particle in three-dimensional volume following the Hill's spherical vertex formulation as described in [18]. One of the positions of the particle is shown in Fig. 3.

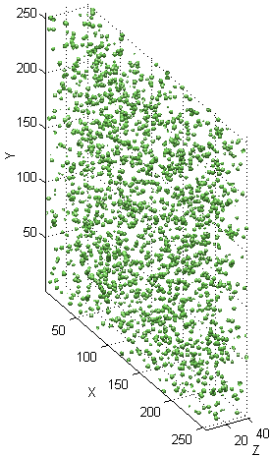

Fig. 3 Synthetic phantom of particle distribution in volume

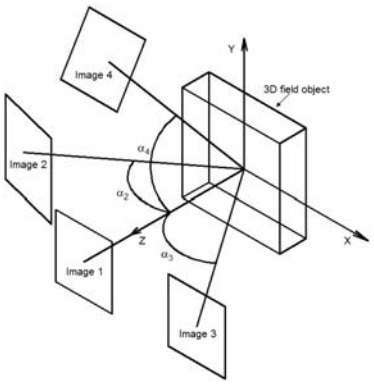

Fig. 4 Positions of projection views corresponding to object field

3.3 Reconstruction performance

Reconstruction errors should be calculated to confirm the discrepancy between the reconstructed result and the actual field. The average error of the reconstructed object function $\hat{f}$ and the reference phantom function f can be obtained as follows [15, 19]:

$$\Phi_{avg} = \frac{\sum_{j=1}^{N} \left| f(x_j, y_j, z_j) - \hat{f}(x_j, y_j, z_j) \right|}{N} \tag{12}$$

The performance of the tomographic reconstruction is also evaluated by recommending the reconstruction quality defined as the normalized correlation coefficient of the exact and reconstructed intensity distribution [11]:

$$Q = \frac{\sum f(x_j, y_j, z_j).\hat{f}(x_j, y_j, z_j)}{\sqrt{\sum f^2(x_j, y_j, z_j).\sum \hat{f}^2(x_j, y_j, z_j)}} \tag{13}$$

4. Reconstruction results and discussion

4.1 Droplet distribution

The MART was tested with several basis functions such as B-spline, cosine and Gaussian. The computer-synthesized test phantoms were assumed to be distributed in the volume of *15x15x15*. In order to avoid losing data, each two-dimensional projection of this object contains 20x20 pixels or line-of-sight. The center of the 3D object was assumed as the global coordinate and the local coordinate of each projection was calculated according to the global coordinate as shown in Fig. 4. Four projections were positioned in Fig. 4 with $\alpha_1 = 0$, $\alpha_2 = -45^o$, $\alpha_3 = 45^o$ and $\alpha_4 = 45^o$ at different height.

The reconstruction results of droplets are shown in Fig. 5 which shows that shapes and positions of the droplets after reconstructing with 100 iterations of the MART using three basis functions are similar to the real phantoms as shown in Fig. 2. According to these results, the quality and average error were calculated and shown in Fig. 6. This figure indicates that the cubic-cosine basis function yields the highest quality and the lowest average error while the Gaussian basis function gives reverse results with the lowest quality and the highest error in comparing with other functions. These discrepancies were attributed to the distribution of the basis functions as shown in Fig. 1 (b). In the same range of the distances to the center the weighting values increase with different increments. For cubic-cosine and cubic-B-spline, the weighting values jump to the next faster than the Gaussian function. While, as above explanation, the weighting coefficients using a ray-tracing method is not distributed smoothly. Thus, the cubic-cosine and cubic-B-spline seem to be conformable to the object distributing in the narrow size and containing meander shape. It can be cleared by comparison between two reconstructions of the first and the second phantom data as shown in Fig. 5 (a), (b) and (c) which contain the quasi-spherical shape and Fig. 5 (d), (e) and (f) which contain the narrow and meander shape. The lowest reconstruction quality and precision is obtained from the Gaussian function and the results get better from ray-tracing to cubic cosine in which the Gaussian for the first phantom is better than for the second phantom.

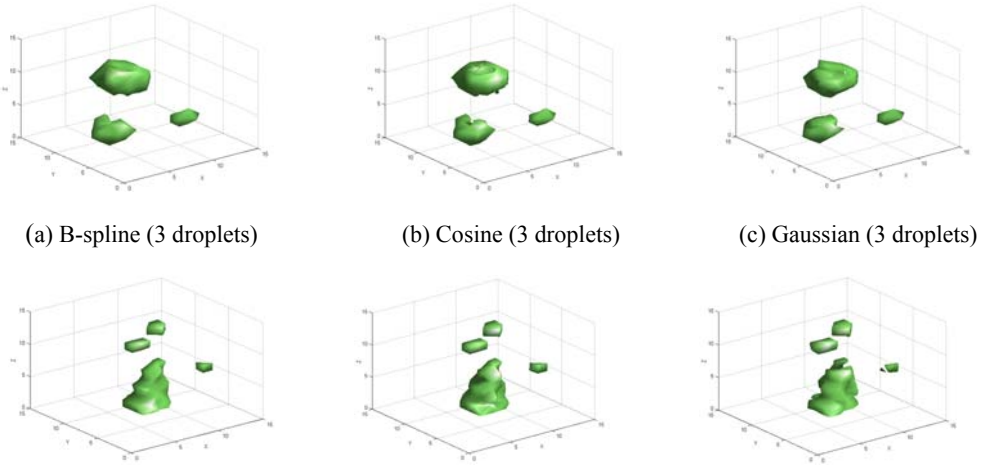

(a) B-spline (3 droplets) (b) Cosine (3 droplets) (c) Gaussian (3 droplets)

(d) B-spline (4 droplets) (e) Cosine (4 droplets) (f) Gaussian (4 droplets)

Fig. 5 Reconstructed results using MART

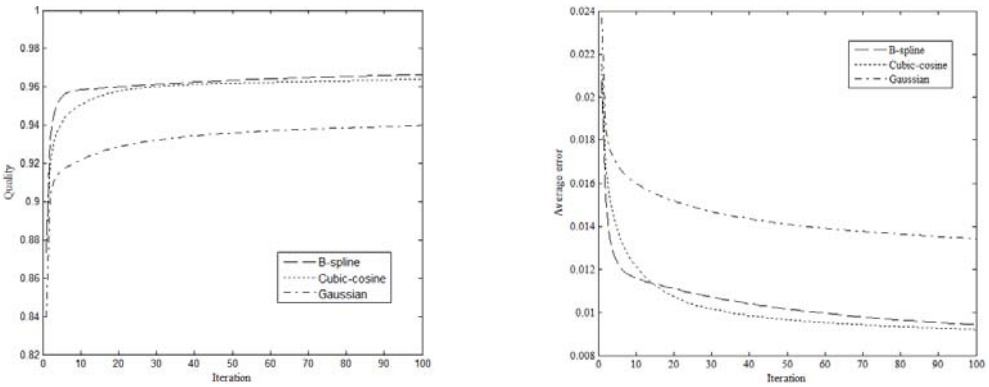

Fig. 6 Quality and average error of reconstruction by MART

4.2 Random particle distribution

The volume of particle was supposedly captured by four cameras placed similarly to the configuration as shown in Fig. 4 to obtain four projections. Each camera has the size of *255x255* pixels and its intensity is computed by using the designed projection matrix and the random intensity generated at each voxel. As aforementioned discussion, the choice of the basis function depends on the shape of the object field needed to be reconstructed. Thus, the Gaussian function was chosen to calculate the weighting values for the third phantom as the smoothly spherical particles in three dimensions. However, to confirm this statement, the cubic-cosine function which produces the highest quality and the lowest average error for droplet reconstruction was also used in this case. Because the particles were distributed in the volume with the size of *255x255x41* voxels, the size of the projection matrix would be very large. This needs much time to calculate and much memory to save the matrix. However, because the matrix is very sparse, the algorithm could calculate and save the non-zero values for each line-of-sight which just cover some voxels of all volume [16].

The MART was also performed with *100* iterations. The reconstructed results are shown in Fig. 7 (a) which is the result for the cubic cosine function while Fig. 7 (b) for the Gaussian function. Figure 7 (a) indicates the limitation of the cubic cosine basis function with many undesirable particles or "ghost particles" [11] occurred paralleling with the true particles. While, Fig. 7 (b) shows better result in which the sizes and the positions of the particles are similar with the real phantom as shown in Fig. 3. The domination of the Gaussian basis function is also pointed out by Fig. 8 that shows the average errors measuring from the real data and the reconstruction data. Figure 8 shows the lower error for the Gaussian function than for the cubic cosine function. The results indicate that the MART using the Gaussian basis function for forming the weighting values of the projection matrix to reconstruct the Gaussian random particles distribution obtains good reconstruction quality and precision.

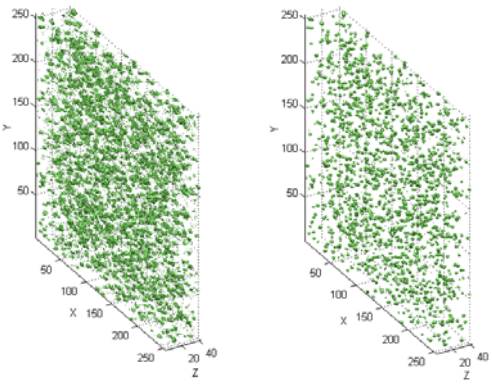

(a) Cubic cosine function (b) Gaussian function

Fig. 7 Reconstructed results of particle distribution

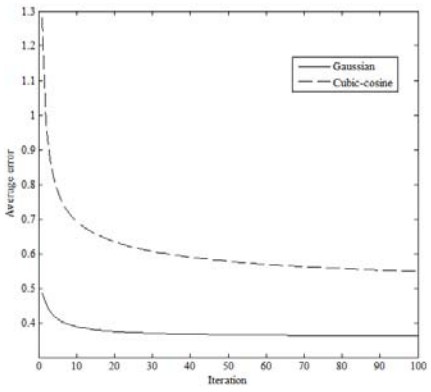

Fig. 8 Average error of reconstruction for particle distribution

4.3 Three-dimensional cross-correlation for three-dimensional velocity vector

In order to perform the cross-correlation to test the quality of the reconstruction with two different basis functions, a synthetic 3D flow would be created basing on the displacements of the particles. Using Eq. (11) the *2580* particles were

generated randomly in the volume of *255x255x41* voxels as the first position. The second position would be defined by measuring the displacement of each particle in three-dimension. In this study, the Hill's spherical vortex is used as the reference flow field. The calculating process of particle velocities and the displacements is described in [18] with the induced velocity given as $u_0 = 1m/s$ and the diameter of the vorticity containing sphere given as $a = 50$ voxels in this study. With two three-dimensional volumes of the particle flow at time t and $t + \Delta t$, the three-dimensions and three-components of velocity vectors can be obtained by using the three-dimensional cross-correlation [17, 18].

According to the phantom, the cross-correlation result is shown in Fig. 9 (a) that is a pattern to evaluate the quality of the reconstruction results. The cross-correlation result as shown in Fig. 9 (b) is the result using the reconstructed volume with Gaussian basis function. This seems to be good fit with the result using the real data as shown in Fig. 9 (a) clearly distinguished with the lower quality as shown in Fig. 9 (c). The uncorrect field vectors in Fig. 9 (c) are due to many ghost particles generated after reconstructing.

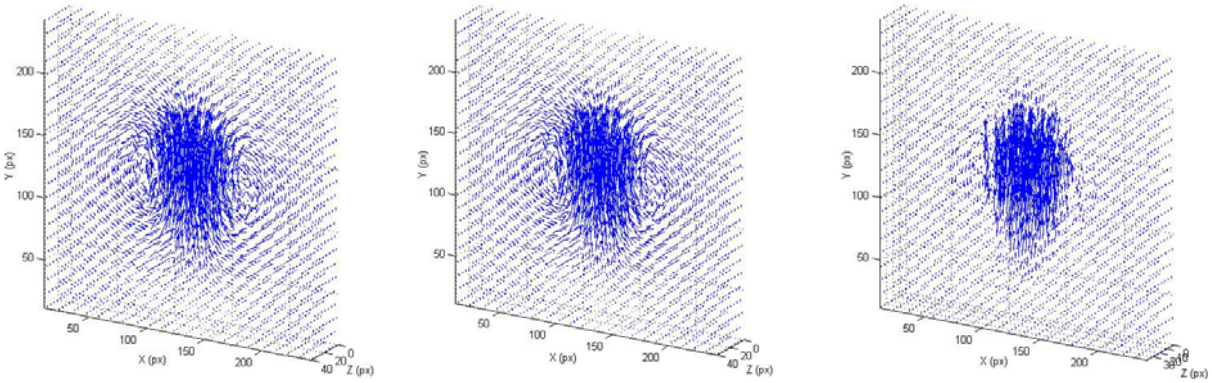

(a) Real phantom (b) Gaussian reconstruction (c) Cubic cosine reconstruction

Fig. 9 Velocity vectors using three-dimensional cross-correlations

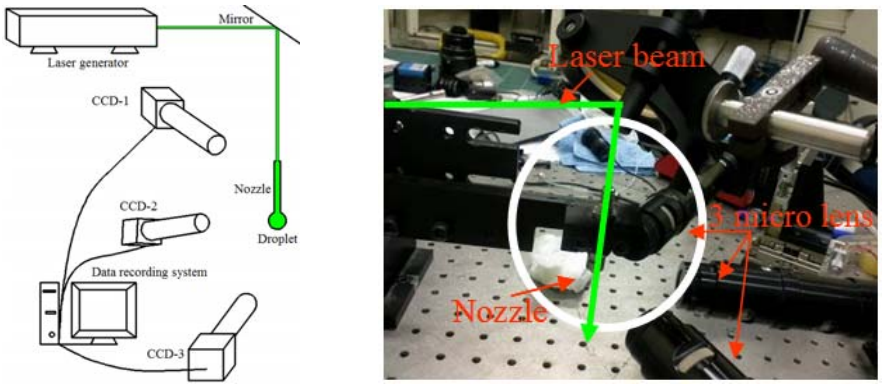

(a) Schematic and photo of experimental arrangement

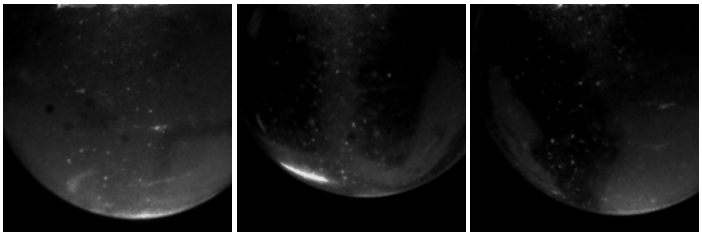

(b) Recorded images from three cameras

Fig. 10 Experimental setup for tomographic PIV

5. Reconstructed results from experimental images

5.1 Experimental setup and captured images

In order to test the appropriation of the Gaussian basis function combining with the MART algorithm, an experiment was performed using three CCD cameras with a resolution of 500x500 pixels to record the images of the moving particles inside the ejected droplet simultaneously. Three cameras were mounted as shown in Fig. 10 (a) with the angle between CCD-1 and CCD-2; CCD-2 and CCD-3 of 60°. A laser beam which was generated from a 5W Ar-Ion Laser (Lexel) was directed through the nozzle to the inner of the droplet to illuminate the whole droplet. The operating fluid was distilled water, and the fluorescent particles were (1μm) seeded in this experiment. The drops were dripped by the gravitational force and the recorded images of particles inside the drop from three cameras are shown in Fig. 10 (b).

5.2 Reconstruction result using experimental images

Figure 11 (a) shows a small volume in which two reconstructed volumes from the images at time *t* and *t + 0.03s* are overlapped. The size of the reconstructed volume was *255x255x41* voxels. The image processing steps were performed for the recorded images. These steps included temporal image processing, spatial filtering and Gaussian smoothing. Although the reconstruction accuracy cannot be evaluated because of the experimental projections, it just can be evaluated by comparing the particles in the projection images with the reconstruction volume. The result was reasonable as looking the positions of particles in images and inside the volume. Thus, these two volumes of particles were used to complete the three-dimensional cross-correlation [18] as shown in Fig. 11 (b). Since the directions of velocity vectors were similar with the particle motions in the movies, the reconstruction accuracy was supposed to be acceptable.

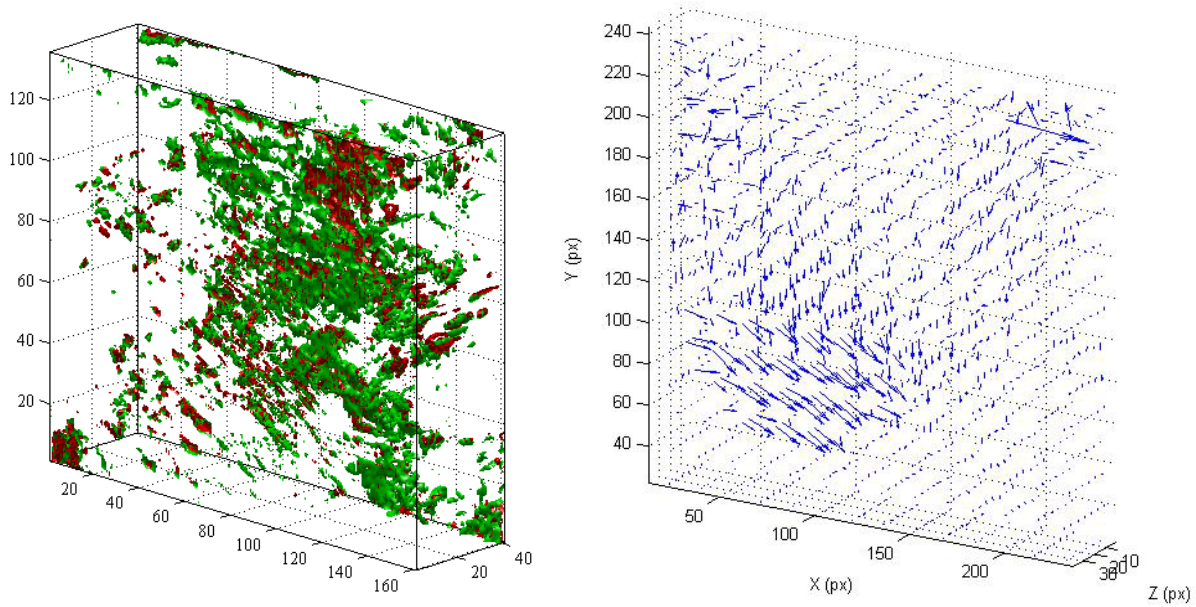

(a) Iso-surface of particles (red-first, green-second) (b) Three-dimensional velocity vector field

Fig. 11 Three-dimensional reconstructed results from experimental images

6. Conclusion

The MART algorithm was examined by using three basis functions for building the projection matrix. The algorithm illustrated its reliability and quality through numerical evaluation using several kinds of the computer-synthesized test phantoms. The numerical performances indicated that the cubic functions as cosine and B-spline are appropriate with the tomographic reconstruction of the field objects containing narrow size and meander shape while Gaussian basis functions show good quality and precision for the tomographic reconstruction of the field objects containing the quasi-spherical and spherical shapes.

The algorithm presented in this study was proposed as a promising tool to analyze the ejecting behaviors of the droplets and the multi-jetting from the menisci of liquid under the electric field using the intensity of the two-dimensional images from the calibrated cameras as the projection data. Furthermore, with high quality of reconstruction, the algorithm can also be applied in reconstructing the particle field volumes preparing for the three-dimensional cross-correlation to obtain the three-dimensions and three-components of the velocity vector in complex flows such as turbulent and vortex flows.

Acknowledgement

This work supported by the Basic Science Research Program through the National Research Foundation of Korea (NRF) funded by the Korean government (MEST) (No. 2011-0023457).

References

1. Park J.U., Hardy M., Kang S.J., Barton K., Adair K., Mukhopadhyay D.K., Lee C.Y., Strano M.S., Alleyne A.G., Georgiadis J.G., Ferreira P.M., Rogers J.A., *High-resolution electrohydrodynamic jet printing*, Nature Materials Vol. 6 782 – 789 (2007).
2. Luedtke W.D., Landman U., Chiu Y.H., Levandier D.J., Dressler R.A., Sok S., Gordon M.S., *Nanojets, electrospray, and ion field evaporation: molecular dynamics simulations and laboratory experiments*, J Phys Chem A. 112 (40) 9628-49 (2008).
3. Jaworek A., Sobczyk A.T., *Electrospraying route to nanotechnology: An overview*, J. Electrostatics 66 197-219 (2008).
4. Jaworek A., Krupa A., *Jet and drops formation in electrohydrodynamic spraying of liquids*, Exp. In Fluid 27 43-52 (1999),
5. Wan X., Yu S., Gao Y., Zhu Q., *Self-adaptive reconstruction algorithm for emission spectral volume tomography*, Opt. Eng. 43(5) 1244–1250 (2004).
6. Mishra D., Longtin J. P., Singh R. P., Prasad V., *Performance evaluation of iterative tomography algorithms for incomplete projection data*, App. Opt. Vol. 43, No. 7, pp. 1522-1532 (2004).
7. Kak A.C., Slaney M., *Principles of Computerized Tomographic Imaging*, IEEE Press, New York, (1987).
8. Verhoeven D., *Limited-data computed tomography algorithms for the physical sciences*, App. Opt 32 3736-3754 (1993).
9. Gordon R., *A tutorial on ART*, IEEE Trans. on Nucl. Science, NS-21, 78-92 (1974).
10. Gordon R., Herman G. T., *Three-dimensional reconstructions from projections - review of algorithms*, Int. Rev. Cytol. 38, 111–151 (1974).
11. Elsinga G. E., Scarano F., Wieneke B., Oudheusden B. W. van, *Tomographic particle image velocimetry*, Exp Fluids 41:933–947 (2006).
12. Petra S., Schröder A., Schnörr C., *3D Tomography from few projections in experimental fluid dynamics*, in Imaging Measurement Methods for Flow Analysis Vol. 106, pp. 63-72 (2009).
13. Hanson K.M., Wecksung G.W., *Local basis function approach to computed tomography*, App. Opt. 24(23), 4028-4039 (1985).
14. Wan X., Gao Y.Q., Yu S.L., *Limited-view tomography algorithms for plasma diagnostics*, Proc. SPIE 4927 625-633 (2002).
15. Chen C., Kim Y.J., Ko H. S., *Three-Dimensional Tomographic Reconstruction of Unstable Ejection Phenomena of Droplets for Electrohydrodynamic Jet*, Exp. Ther. & Fluid Sci., Vol. 35 (3), pp. 433 – 441 (2011).
16. Atkinson C., Soria J., *An efficient simultaneous reconstruction technique for tomographic particle image velocimetry*, Exp Fluids 47:553–568 (2009).
17. Scarano F., Riethmuller M.L., *Advances in iterative multigrid PIV image processing*, Exp. Fluids Suppl., S51-S60.
18. K. Lynch, *Development of a 3-D Fluid Velocimetry Technique based on Light Field Imaging*, Master thesis, Auburn Uni., (2011).
19. Ko, H.S., Kihm K.D., (1999), *An Extended Algebraic Reconstruction Technique (ART) for Density-gradient Projections: Laser Speckle Photographic Tomography,* Exper. Fluids 1999, 27, pp. 542-550.